UNIVERSITY OF BRISTOL

THIRD YEAR INDIVIDUAL RESEARCH PROJECT

Author:
Edward MCLAUGHLIN

E-mail:
em12509@bristol.ac.uk

Candidate Number:
57182

Supervisor:
Dr. D.DI MAIO

Lead Juror:
Dr. Z.J.JIANG

Moderating Juror:
Dr. J.F.BURN

Experimental Non-linear Device Designs: A double beam and a ring and pillar device

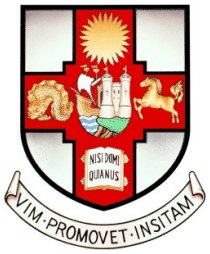

IN PARTIAL FULFILMENT OF THE REQUIREMENTS
FOR THE DEGREE OF
MASTER OF ENGINEERING IN THE SUBJECT OF
MECHANICAL ENGINEERING

April 21, 2015

Acknowledgements

Dr. Di Maio - project supervisor - for proposing, coordinating and overseeing the project, including the set-up of the experiment and experiment design, as well as being my first point of contact for theory related questions. For the duration of the project Dr. Di Maio held frequent progress meetings to provide guidance and feedback.

Bristol University Workshop for the realisation of the two devices, with particular reference to *Ian Plumber* who was my first point of contact in the workshop.

Lab technicians in the dynamics laboratory, with particular reference to *Tony Griffith*, who helped me to adjust and refine my devices, and *Clive Rendall*, who was my first point of contact for technical help in the laboratory in the absence and to the assistance of Dr. Di Maio.

Declaration

The accompanying research project report entitled: "Experimental Non-linear Device Designs: A double beam and a ring and pillar device" is submitted in the third year of study towards an application for the degree of Master of Engineering in Mechanical Engineering at the University of Bristol. The report is based upon independent work by the candidate. All contributions from others have been acknowledged above. The supervisors are identified at the start of the report. The views expressed within the report are those of the author and not of the University of Bristol.

I hereby declare that the above statements are true.

Full Name: EDWARD MCLAUGHLIN

Signed (author):

Date: April 21, 2015

Declaration of Copyright

Certification of ownership of the copyright in a dissertation presented as part of and in accordance with the requirements for the Final Degree of Master of Engineering at the University of Bristol, Faculty of Engineering.

I hereby assert that I own exclusive copyright in the item named below. I give permission to the University of Bristol Library to add this item to its stock and to make it available for consultation in the library, and for inter-library lending for use in another library. It may be copied in full or in part for any bone fide library or research worker on the understanding that users are made aware of their obligations under the copyright legislation, i.e. that no quotation and no information derived from it may be published without the authors prior consent.

Author:	EDWARD MCLAUGHLIN
Title:	Experimental Nonlinear Device Designs: A double beam and a ring and pillar device
Date of Submission:	April 21, 2015

This dissertation is the property of the University of Bristol Library and may only be used with due regard to the author. Bibliographical references may be noted but no part may be copied for use or quotation in any published work without prior permission of the author. In addition, due acknowledgement for any use must be made.

Full Name: EDWARD MCLAUGHLIN

Signed (author):

Date: April 21, 2015

Abstract

The primary aim of this project is to engineer a mechanical device which demonstrates non-linear (NL) behaviour. The device(s) must resonate at least once between the frequencies of 100 Hz to 300 Hz and not have 50% geometric similarity with another student's project. For this project, two devices were manufactured, visible in Figs. 2.2 (double beam device) and 2.3 (ring and pillar device). The response of the each device was measured by sweeping a sinusoidal excitation force in a frequency range between 100 Hz to 300 Hz. Frequency Response Functions (FRFs) were produced as well as circle fits being made to the Nyquist plots of the raw data at the different excitation amplitudes. The frequency range was swept through both forwards and backwards and the device(s) were modified to inspect the effects of different material parts to NL behaviour. The natural frequency and peak resonance amplitudes both varied with excitation force for the ring and pillar device while it also behaved differently depending on the direction of the sweep. The unmodified double beam device maintained the same natural frequency while its resonant amplitude reduced as input force was increased. The modifications made to the double beam device resulted in its natural frequency altering as excitation levels varied.

Contents

List of Figures

Acronyms

NL - Non-Linear
FRF - Frequency Response Function
FEM - Finite Element Modelling
CFD - Computational Fluid Dynamics
DAQ - Data Acquisition

1 Introduction

Often when a physical model is tested, the results do not completely agree with those predicted by the computed model. This can be for various reasons: the experiment may be fundamentally flawed (e.g. experimental process or measurement inaccuracies), the digital model may not be identical to the physical object in geometry or materials or the digital model may not account for all physical phenomena. Even if the first two conditions are satisfied, there are still large steps to be made in computational modelling, prime examples being Finite Element Modelling (FEM) and Computational Fluid Dynamics (CFD). One of the aspects of physics which engineering still struggles to model is NL dynamics. The NL domain of dynamics has few analytical tools in comparison to its counterpart, linear systems. Although for certain amplitude and frequency ranges, many NL systems may be approximated as linear, in reality, no mechanical system is truly linear. As a result, the importance of NL techniques to assess real world problems is growing as engineering systems become increasingly complex. In order to have accurate predictions of how a system will react, it is essential that a better understanding of non-linearities and their effects is developed. One of the main reasons that these techniques are so challenging to develop is that the laws of superposition of modes are not applicable to these systems. Moreover, there exist phenomena such as bifurcations, modal interaction and internal resonances which create complications for obtaining any omni-applicable laws or sets of equations for NL systems.

Once a comprehensive understanding of NL behaviour is achieved it won't only allow engineers to avoid errors which linear systems invoke, but it will permit the creation of more accurate modelling systems such as FEM, CFD and other dynamics modelling tools. The exploitation of NL dynamics can aid industry by avoiding design over-specification, which will result in expensive manufacturing, or under-specification of designs, which will not perform sufficiently and in certain cases become unsafe. For example, if the grip of a car's tyres is assumed to be independent of the area in contact with the road then a car manufacturer may end up engineering tyres out of an expensive material with a very high specification. However, the equation often given for friction, $Fr = \mu N$ is not always reliable. This is because there are many NL aspects to grip, for example the apparent contact area of the tyre is not the same as the actual contact area due to asperities on the surfaces of the tyre and the road. Furthermore, the coefficient of friction μ between the tyre and the road is likely to change as the car turns a corner and the tyre heats up.

This report assesses the non-linearities of two engineering devices; a double beam device and a ring and pillar device. Both devices were tested using the same equipment and by the same means, detailed in the "Materials and Method" section of this report. The response is analysed for a frequency range of 100 Hz to 300 Hz at different excitation forces as well as using a forwards ("step-up") and backwards ("step-down") frequency sweep and adapting the models, observing any response changes.

The purpose of this report is not to give a mathematical insight in NL dynamics but to explore the devices experimentally in order to highlight the devices NL characteristics and to arrive at qualitative conclusions as to why certain phenomena occur through the use of simple quantitative graphing techniques. It is also important to stress that each device is being used as a

tool to highlight sources and characteristics of NL behaviour. Therefore, the discussion on each device will not be fully comprehensive or comparatively identical with the other. Instead, from the experimental results, certain behaviour which is best highlighted by either or both devices will be discussed in their respective section and where relevant compared or contrasted to the other device.

1.1 Sources of Non-linearity

Non-linearities can arise from an array of different sources; complex geometry, bolts and other types of fasteners (Eriten et al., 2013), temperature changes (Lagoudas et al., 2005), natural phenomena e.g. coulomb friction, changes in boundary conditions of the system and large displacements beyond the linear regime (Wilcox, 2014).

The example of a spring is often taken; Hooke's law tells us that displacement, x is proportional to force, F, which a constant of proportionality, k, i.e.

$$F = Kx \tag{1}$$

While this holds true for relatively small values of x, as displacement increases, the amount of force per unit length displaced increases significantly. Expressed differently, the amount of energy needed to be exerted on the system to displace the spring by a unit length increases as total displacement increases.

$$\frac{dF}{dx} \neq const. \tag{2}$$

This is due to the inherent geometry of a spring. Higher or lower order terms must be added to Eq. 1 in order to account for this NL phenomenon (these added terms don't have to be power terms, they can be exponential, polynomial or logarithmic terms), giving

$$F = ax^m + ... + bx^{1/3} + cx^{1/2} + Kx + \alpha x^2 + \beta x^3 + ...\gamma x^n = F(x) \tag{3}$$

If we take the original example about grip on a tyre, we can better describe the relationship between friction, speed and contact area if we know higher or lower order terms i.e.

$$Fr = aN^m + ... + bN^{1/3} + cN^{1/2} + \mu N + \alpha N^2 + \beta N^3 + ...\gamma N^n = Fr(N) \tag{4}$$

This project is concerned with investigating NL behaviour in mechanical devices found while exciting structures with complex geometry, bolts and mechanical devices, in this case aluminium arches which act as springs.

1.2 Assessing and Measuring Non-linearities

There are many different graphing tools which can demonstrate the non-linearity of a structure. The two which will be used in this report are FRFs and Nyquist plots, and further data which may be extrapolated from these graphical techniques such as damping ratios.

FRFs plot the receptance (displacement transfer function), mobility (velocity transfer function) or inertance (acceleration transfer function) against excitation frequency, explicitly showing the natural frequency of a structure and how this may change with excitation force. For a linear system, the shape of the amplitude peak is symmetrical about the natural frequency and the natural frequency will be the same for all excitation forces, with the response amplitude changing in proportion to the change in excitation force. For a NL system, the FRF is unlikely to be symmetrical about the natural frequency and the natural frequency is unlikely to be the same for all excitation frequencies creating a spine effect - a line connecting all of the natural frequency peaks. The characterisation of the non-linearity of a device ingrained in an FRF is in the shape of this spine, the symmetry or anti-symmetry of the response about the natural frequency and the relationship between peak amplitude and input force.

Nyquist plots are a further tool to determine the linearity of a response. The plot of the real and imaginary parts of a linear response has various qualities; it is circular, its radius will increase linearly with excitation force, and finally, if excited at a set of excitation forces, the lines connecting a given frequency point on each response will be straight. Deviation from these qualities of linear Nyquist plots can be seen as signs of non-linearities present in the structure.

1.3 Literature Review

Siller (2004) develops novel methods of system identification - explicit formulation (EF) and hybrid model technique (HMT) - localising and characterising non-linearities for large structures. The methods are explicitly applied to two sources of nonlinearity; cubic stiffness and friction damping. The first technique, EF, takes physical properties and predicts the FRF based on these properties. When compared with test results, this method demonstrates reasonable accuracy. The second technique, HMT, is an alternate take on current NL modal analysis techniques, using generalised modal coordinates to describe the linear system, keeping the NL components in the physical domain, hence hybrid model technique.

In Amabili (2004) the data sets found experimentally for a plate subject to harmonic radial excitation while the plate is constrained by three different types of boundary condition are compared with a NL numerical model derived in the paper. It is found that there is agreement between the experimental data and the numerical results close to the resonant frequencies of the plate under each boundary condition.

Kerschen et al. (2005) discusses the past and recent developments in NL system identification. The most popular methods of system identification and numerical analysis are examined using theory and practical example. Their limitations and advantages are then assessed to identify promising future research areas. The majority of this paper is outside of the scope of this project as it is quite mathematically advanced. However, the paper does demonstrate the basics of non-linear graphical analysis, including FRFs. The means by which non-linearity can be manifested are also explained, for example a response may change depending on if the excitation was an up-step or down-step signal (i.e. if the response is path dependant or not) and the appearance of 'tongues' in frequency - energy plots, which signify the transfer of energy between modes.

Fig. 1.1 demonstrates the softening (leaning backwards) behaviour of NL structures whose

natural frequencies reduce as excitation force increases. Equally, some systems demonstrate hardening behaviour, an increase in spring stiffness as force increases, resulting in an increase in natural frequency (leaning forward). The difference in response depending on an up-step or a down-step is also displayed in Fig. 1.1, this shows graphically the concept of path dependency of the response of NL systems. That is, does the response of a mechanical system depend on how the structure has previously been excited? Kerschen et al. (2005) also suggests a system identification procedure which can be seen in Fig. 1.2. This procedure follows three stages: detection, characterisation and parameter estimation. This report will be concerned with these steps up to characterisation, in particular determining the nature of the nonlinearity.

G. Kerschen et al. / Mechanical Systems and Signal Processing 20 (2006) 505–592

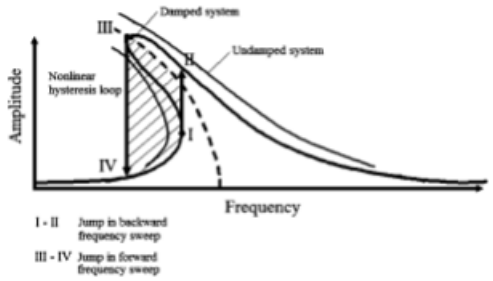

Fig. 5. Nonlinear jump phenomena in the fundamental resonance of a mode with softening cubic nonlinearity.

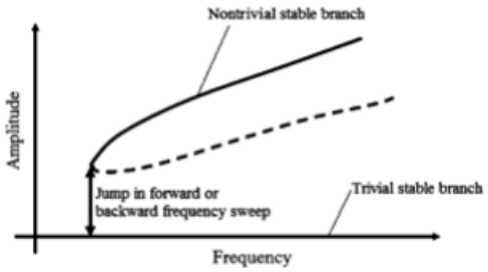

Fig. 6. Nonlinear jump phenomenon in the subharmonic resonance of a mode with stiffening cubic nonlinearity.

Figure 1.1: Softening behaviour and path dependence

Lagoudas et al. (2005) is a report which assesses the non-linearities of shape memory alloys and closely matches the report we must do for our project. It is a technical report of an experiment using accelerometers to observe the non-linearities of a structure made from shape memory alloy. The structure is first analysed using FEM capabilities. The experimentation results are then plotted; acceleration, temperature, natural frequencies etc. Temperature is plotted as shape memory alloy works using temperature differences to deform and reshape itself. An extensive mathematical modelling of the system is then performed, which is beyond the scope of this project.

Link et al. (2011) investigates possible tools for NL analysis with the purpose of proper and robust design for satellite parts. Frequency (FRFs) and time domain techniques are explored, as well as interpolation techniques to estimate unmeasured excitation forces. This is extremely useful as it allows the response of a structure under conditions not necessarily possible in the lab to be estimated. The method of interpolation was seen to work well between found data points, however, it was not deemed useful for excitation forces outside of the upper and lower

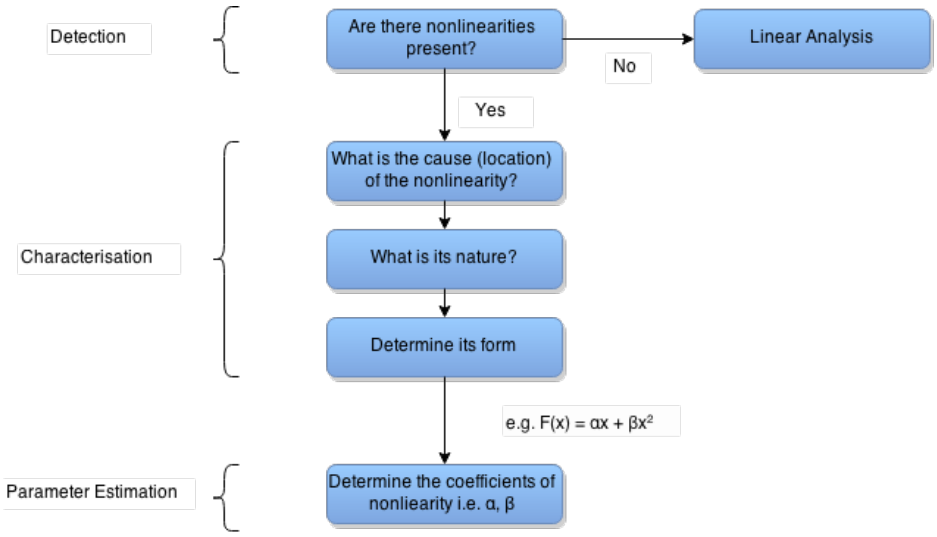

Figure 1.2: System identification

bounds of excitation frequencies which had been tested. Furthermore, argand diagrams are used to assess the linearity of a response. By plotting the imaginary and real parts of the response for different levels of excitation it is possible to see how the measure responses differ from the predicted linear response. It is asserted that a linear system will have a circular shape. Moreover, if the points for a given frequency on each response circle are joined together, the line will be straight for a linear model. An example of a linear and NL argand diagram is shown in Fig. 1.3 (Link et al., 2011).

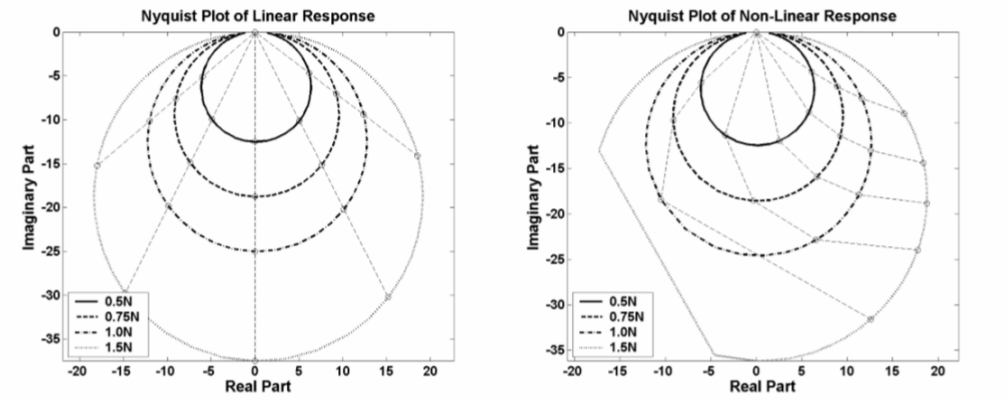

Figure 1.3: Linear and nonlinear Nyquist examples

Eriten et al. (2013) is an investigation into the NL dynamics introduced to a system which incorporates bolts, welds or rivets with the primary example taken being a bolted beam. This is done using NL system identification techniques which incorporate the theory of empirical modal decomposition (EMD) (using Hilbert transform), NL interaction models (NIMs) and intrinsic modal oscillators (IMOs). By identifying the intrinsic mode functions (IMFs) using EMD, the dominant IMFs may be found using wavelet transforms, sifting out the unimportant IMFs but maintaining accurate system analysis. Then by processing the IMFs using the Hilbert transform, the slow flow dynamics may be found. An example of a two degree of freedom coupled linear

oscillator is analysed using the method mentioned above to confirm its validity. While the theory of this paper is far outside the complexity of this project, it isolates the effects of a bolted joint on the response of a structure, explicitly showing how bolted joints affect FRFs.

Roth et al. (1942) is a report assessing the frictional properties (both static and dynamic) of rubber. The specimens were prepared especially for the experiments conducted, with varying surface roughness. They were then incrementally inclined until slip occurred at which point static friction was calculated and once slip occurred, dynamics friction was investigated. The main plot linked with dynamic friction was speed vs friction coefficient. The principle findings from this was that the coefficient of friction increased as speed increased. It was also shown that the discrepancy between two sets of their results was due to the motor vibration. Once this was quelled, the discrepancy was minimised. This showed that vibration (such that rubber might be subjected to in this project or at sealed joint in industrial context) reduced the coefficient of friction for every given test.

2 Materials and Method

For this project, two devices were made for testing, which may be seen in Figs. 2.2 and 2.3. Both devices are made from aluminium 6082-T6 with the following mechanical properties $\rho = 2.70 g/cm^3$, $E = 70 GPa$ and tensile strength, $\sigma_t = 260 MPa$ (Aalco, 2013).

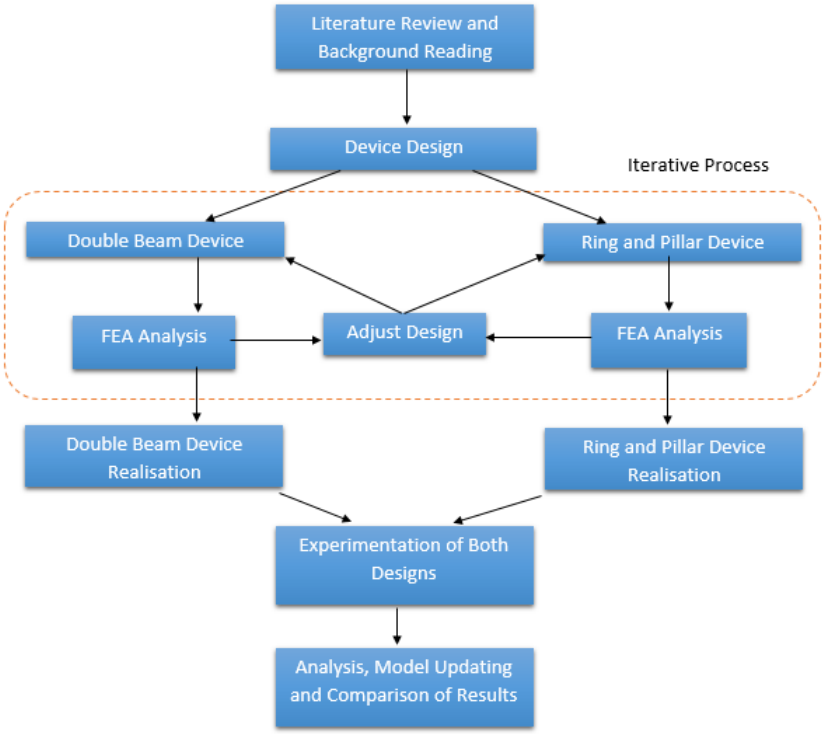

Figure 2.1: Project flow chart

Fig. 2.1 is a flow chart of the project ordered chronologically. It is based on the Pahl and Beitz design model (McMahon, 2014) with a cyclical step a the FEM design stage. The three preliminary design stages: task clarification, specification and concept, were all addressed in the initial meetings with the project supervisor and developed throughout the literature review. The preliminary layout stage was used to produce several initial designs and select the best two for definitive layout through a cyclical process using FEM software as an aid. At this stage it was seen that the natural frequency estimation quickly converged with number of elements and was relatively insensitive to the number of elements past a reasonable amount. Once satisfactory results were achieved when comparing the FEM results with the agreed specification, 3D printed models were made in plastic to present to the project supervisor to confirm the designs were of appropriate scale and fit the project specification and concept previously agreed. The final engineering drawings and CAD models were supplied to the workshop to be realised in 6082-T6 aluminium. Once the designs were realised testing at several different excitation levels was conducted. Both step-up and step-down simulations were made and the models were adapted with various materials and the new response was observed.

The two designs were chosen on the basis of sources of non-linearity, adaptability, variability

and manufacturability. Where adaptability concerns tuning the device to meet the project specification i.e. a resonant peak between 100 Hz to 300 Hz, variability is the possibility to change the device to vary its response e.g. rubber partitions and manufacturability is ease of manufacture. Values between 1 and 10 (10 being most agreeable) were assigned to each device for each property. The two devices were selected on a combination of total score and sources of non-linearity. Table 1 shows the selection process.

Table 1: Device Selection Process

Device	NL Source CG[1]	NL Source BC[2]	NL Source MC[3]	Adaptability	Variability	Manufacturability	Total
Double Beam	✓	✓	X	8	7	7	**22**
Saddle	✓	X	X	6	3	3	12
Ring and Pillar	✓	✓	✓	8	7	6	**21**
Mass and Spring	X	X	✓	8	5	7	20

2.1 Double Beam Set-up

The double beam device and its meshing is shown in Fig. 2.2, the image was rendered using Autodesk Simulation Machanical's inbuilt 'colour by face' tool. Two identical aluminium beams are layered on top of a 20 mm aluminium cube. The assembly is bolted together through untapped holes using an M6 bolt leaving an excess of 5 mm of thread in order to attach the device to the shaker table. This was modelled by constraining the interfaces between the parts down the central column in all translation and rotation directions.

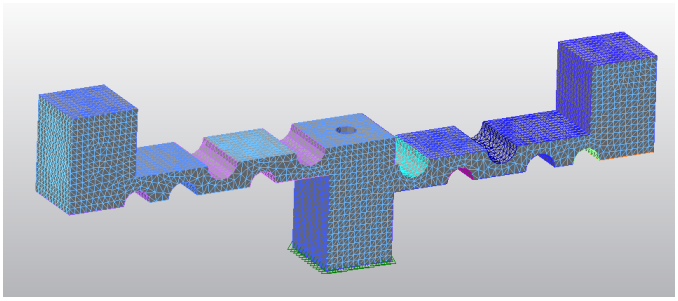

Figure 2.2: Double beam device and mesh (from AutoDesk Simulation Mechanical)

The beams used have semi-circular cut extrusions for two purposes; firstly to weaken the flexural stiffness of the beam and create a more complex geometry, and secondly, to allow for adaptivity, for instance, by inserting parts with different material properties thereby both adjusting the stiffness of the beam and making the stiffness of the beam inhomogeneous.

The device was designed using Autodesk Inventor, while Autodesk Simulation Mechanical

[1]Complex geometry
[2]Bolted connections
[3]Mechanical components i.e. springs or dampers

was used to estimate the mode shapes and resonant frequencies of the device. An iterative design process, as can be seen in Fig. 2.1, was used for the beams, adding additional weight onto the end of the beam according to the equation $\omega_n = \sqrt{k/m}$ until satisfactory resonant frequencies were achieved within the desired frequency range of 100 Hz to 300 Hz.

2.2 Ring and Pillar Set-up

The ring and pillar device and its meshing is shown in Fig. 2.3, the image was rendered using Autodesk Simulation Machanical's inbuilt 'colour by face' tool. This device is made up from two identical aluminium pillars which were bolted to two identical aluminium strips (147 mm x 22.5 mm x 1.5 mm) each with two ellipses (40 mm x 12 mm) extruded out of them. The assembly was bolted together using M4 bolts and nuts through untapped holes. The pillars have semi-circular cut extrusions for the same two purposes discussed for the beams in the previous device.

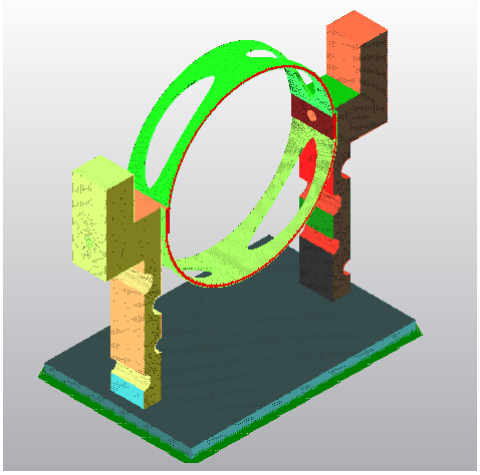

Figure 2.3: Ring and pillar device and mesh (from AutoDesk Simulation Mechanical)

The device was designed using Autodesk Inventor, while Autodesk Simulation Mechanical was used to estimate the mode shapes and resonant frequencies of the device. These mode shapes and resonant frequencies are shown in Fig. 2.7. The design was an iterative process, adding mass to the top of the pillars until satisfactory natural frequencies were achieved in the FEM mode shape analysis.

2.3 Testing

A schematic of the set-up of the testing equipment may be seen in Fig. 2.4. A full list of the equipment used can be found in the appendix.

The signal generator, which is controlled by the LabView software via the junction box, generates a step signal which excites the vibration plate to which a given device is attached using M6 bolts. The gain value on the signal generator was set to 1 for all experiments - all excitation signal amplitude changes were made on the LabView software as digital gain adjustments are

more accurate than an analogue dial. The two sensors were waxed onto the end masses of the pillars or beams of each device respectively. These sensors are connected to a Kistler box which amplifies the output response signal. The amplified signal is then fed into a junction box which is connected to the computer and processed by the LabView software. The output signal is displayed on a standard oscilloscope while the signal data is saved into .DAT and .FRF files.

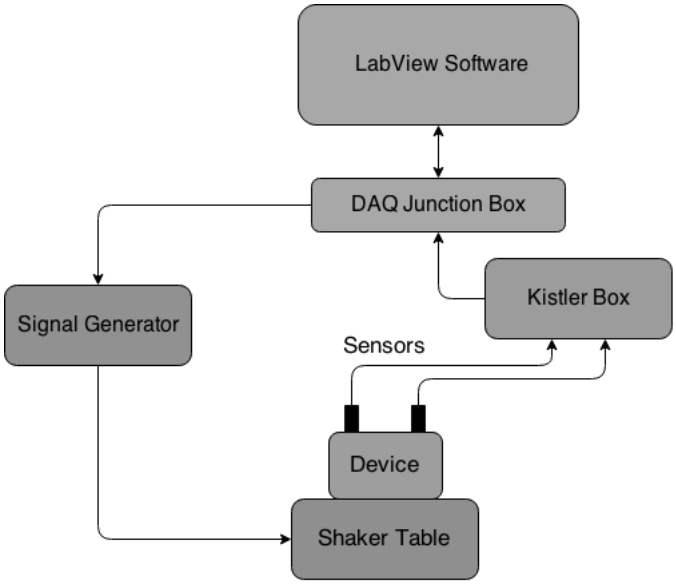

Figure 2.4: Experimental set-up

The devices were subject to six different excitation voltages; 0.10 V, 0.25 V, 0.50 V, 0.75 V, 1.00 V and 1.25 V for the double beam device and 0.25 V, 0.50 V, 1.00 V, 1.50 V, 2.00 V and 3.00 V for the ring and pillar device. The reason for two different sets of excitation voltages was that the wax was not able to withstand the acceleration of the double beam response at greater voltages, resulting in the sensors detaching from the device.

For each device, under each condition (e.g. step-up, step-down, added materials) a sweep of the full 100 Hz to 300 Hz range at 1 V excitation voltage, with a frequency step resolution of 1 Hz, was made before looking closer at interesting frequency ranges with a higher resolution sweep of 0.5 Hz and varying excitation voltages. This allowed the frequency range(s) with peak resonances to be located. Between each experiment the bolts attaching the device to the shaker and any other bolts and nuts in the device were tightened in order to ensure consistency in the experiment set-up.

For the ring and pillar device an analysis of its model shape was made using a laser. This was done by exciting the device with the same sine sweeping signal as before. Various points on the device were picked up by the laser and monitored during the test. The software then used the movement of these points to detect resonant peaks in displacement, and hence, find the natural frequencies. The natural frequency detected in the range of 100 Hz to 300 Hz was 277 Hz. This differs to the other results and the model due to destructive testing previous to the laser test which altered the dynamics of the structure.

2.4 Model Updating

2.4.1 Double Beam Device

For the model updating of the double beam device, the mechanical properties of the aluminium in the FEM package were modified to match the material used. In the physical model the hole for the centre bolt was increased from ⌀4 mm to ⌀6 mm so that device could be fixed onto the top plate of the vibration table, this was then adjusted in the model to match. Finally, an extra 7.5 g was added to the end of the beams in order to account for the weight of the accelerometers. The model updated mode shapes and resonant frequencies are shown in Fig. 2.6.

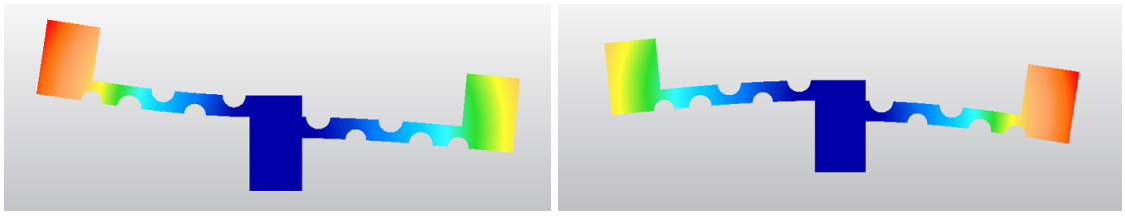

(a) Mode 1: 249.7 Hz (b) Mode 2: 255.5 Hz

Figure 2.5: Double beam device: mode shapes and estimated natural frequencies

The device was then modelled with the rubber partitions. The material properties used for the rubber were: $\upsilon = 0.48$ and $E = 30Gpa$. The natural frequencies for the first mode went from 249.7 Hz to 177.7 Hz and for the second mode went from 255.5 Hz to 233.7 Hz.

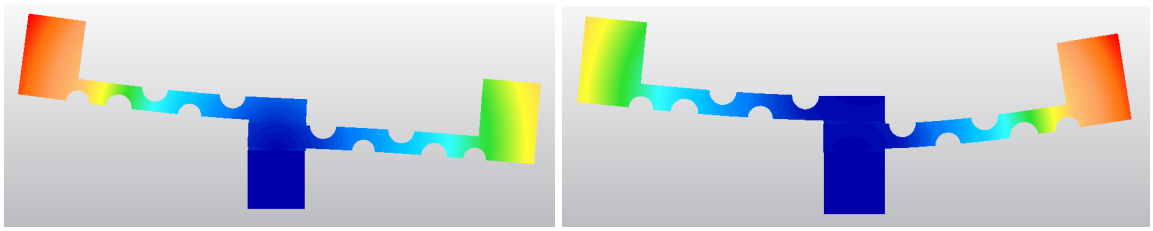

(a) Mode 1: 177.7 Hz (b) Mode 2: 233.7 Hz

Figure 2.6: Double beam device with rubber partitions: mode shapes and estimated natural frequencies

The model was not updated to consider the variation with wire inserts for two reasons, the response of this variation was very similar to the original device (as will be seen in the results results section) and due to the difficulty of modelling the wire inserts on the FEM package used as a result of the variety of materials within the wire cable.

2.4.2 Ring and Pillar Device

As for the double beam model, the mechanical properties of the aluminium were updated in the FEM package. An adaptor plate was made for the pillar-and-ring device in order to attach it to the vibration table. The 108 mm x 79 mm x 5 mm plate was made from 6082-T6 aluminium. The feet of the pillars were screw into the adapter plate using M4 counter sunk bolts. This

plate was in turn attached to the shaker table using M6 bolts. The plate added 117.7 g to the mass of the device and the bottom face was constrained in all translation and rotation directions. 7.5 g was added to each pillar to adjust for the weight of each sensor. This changed the natural frequency of the device as seen below. The new natural frequency is much closer to the natural frequency discovered experimentally ($\approx$ 163 Hz).

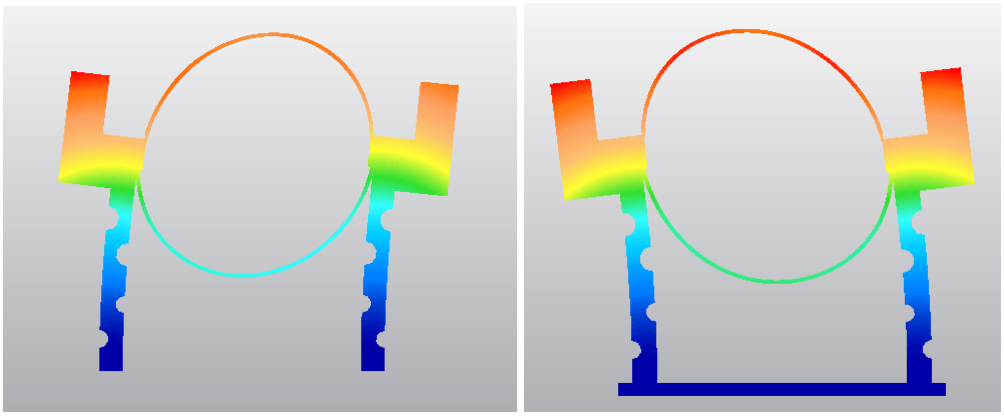

(a) Original natural frequency: 279.8 Hz

(b) Model updated natural frequency: 259.1 Hz

Figure 2.7: Pillar and ring estimated natural frequencies

3 Results

For all test results it is assumed that there is only one degree of vibration. For the double beam device that is considered to be the vertical axis while for the ring and pillar device that is assumed to be the horizontal axis. It is also assumed that there is no rotation in any of the parts and that the bolts do not loosen during testing. Furthermore, it must be noted that the input force is at no point measured and that all FRFs plotted using input voltages. This is due to the fact that the gauge thread is too weak to withstand high levels of excitations, which are required for NL analysis. The author is aware of the loss of information regarding the force but that was considered acceptable as it is likely to be a consistent transfer function which relates voltage supplied to the shaker and the force exerted by the shaker. It was also noted that the two sensors used have different sensitivities (98.5 mV/g and 96.5 mV/g). Although this was taken into account while plotting the two sensors' responses in Fig. 5.1, for all other graphs only the sensor with the higher sensitivity was plotted. It was also necessary to be careful to wax the sensors to their correct beam or pillar in order to have consistent results over separate lab sessions, as the devices are asymmetrical. The response of the two sensors on each device at 1 V for the frequency range 100 Hz to 300 Hz is shown in the appendix, Fig. 5.1. For both devices the responses in the two sensors is very similar. The slight variation may be put down to the asymmetry of the two devices.

3.1 Double Beam Design

Fig. 3.1 shows the receptance FRF of the double beam device for various excitation forces, normalised by the excitation voltage of the response with the highest magnitude, 0.1V. The spine of the responses as well as an estimated single degree of freedom linear response are also shown. The 1DOF linear estimation is made by loading the smallest response curve data (as this made be assumed to be closest to the linear model) into ICATS. This software then gives constants for natural frequency(ω_n), loss factor(η) and the modal constant as magnitude (Mag) and phase (ϕ). Given that:

$$\text{Mag} = \sqrt{a^2 + b^2} \tag{5}$$

$$\phi = tan\left(\frac{a}{b}\right) \tag{6}$$

the constants a and b may be found, where a and b are the real and imaginary parts of the output voltage in complex form such that $Z = a + bi$. Eq. 7 (Ewins, 2000) can then be used to plot the 1DOF linear response.

$$\alpha(\omega) = \frac{X}{V} = \frac{a + bi}{(\omega_n^2 - \omega^2) + \eta i \omega_n^2} \tag{7}$$

It is noticed that the peak response amplitude decreases as excitation force increases. The spine of the responses is in line with the 1DOF linear model and does not infer any softening or hardening behaviour is occurring as the input force is increasing. The spine does begin to bend

forward for 0.10 V in voltage.

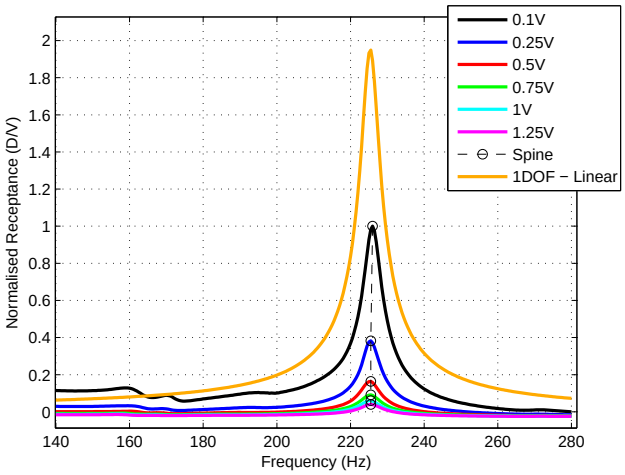

Figure 3.1: Double beam receptance

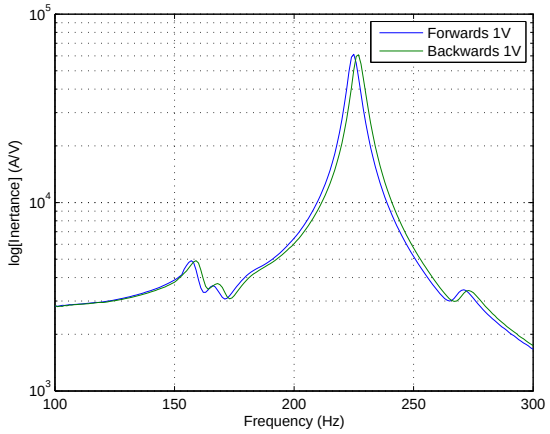

Figure 3.2: Double beam forward and backwards inertance

Fig. 3.2 compares the response of the device to a down-step signal with the response to an up-step signal. The two responses are almost identical except that the response for the down-step resonates at a slightly higher frequency. A more comprehensive analysis of forwards vs backwards response is made for the ring and pillar device.

Fig. 3.3 explicitly demonstrates the relationships between natural frequency, peak amplitude and input voltage for an up-step excitation. The experimental response is compared with the expected linear response. It can be seen that the natural frequency does not vary from a linear model while the peak amplitude is vastly different. The experimental results shows a shape which looks to decay exponentially, whereas the linear model shows a linear increase from 0 to 1 on a normalised scale.

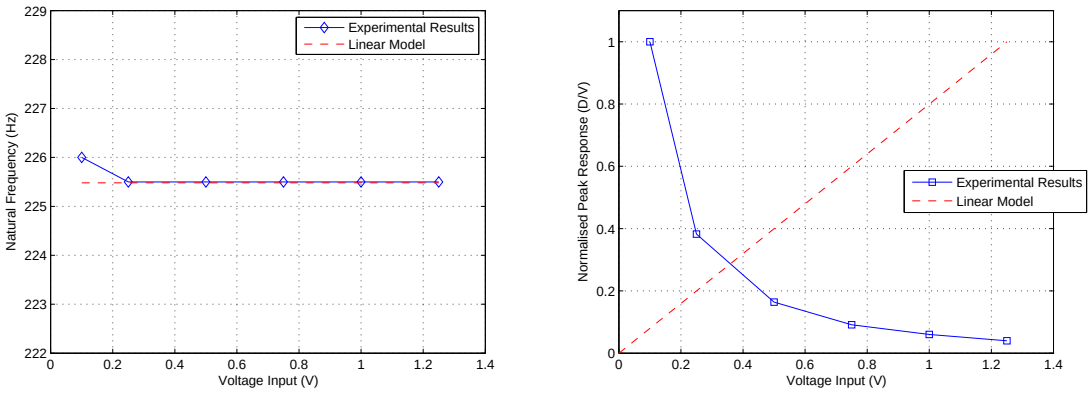

(a) Double beam: natural frequency vs voltage (b) Double beam: peak amplitude vs voltage

Figure 3.3: Beam Natural Frequency and Peak Analysis 140 Hz to 280 Hz

The Nyquist plots in Figs. 3.4 and 3.10 are circle fits of the experimental data. The circle fits are made using the least square method (Gander et al.). It is expected that the Nyquist plots are not scaled realistically, this is because the output signal data was not scaled down taking into account the sensor sensitivity. While this results in unrealistic magnitudes, the shape, phase and relative magnitude all still hold true. The full set of Nyquist plots including the raw data plots are shown in the appendix (Figs. 5.2 - 5.5).

The circle fits in Fig. 3.4 (a) resemble circles on an even axis which reduce in magnitude as input voltage increases from 0.1 V to 1.25 V as with the FRF plot. The lines in Fig. 3.4 (b) which join frequency points on the Nyquist plots for different excitation responses are not straight. The 225 Hz frequency, and its 'path' as voltage is increased, is highlighted in black to demonstrate this phenomena. This signifies that the phase of a given frequency is not the same for different levels of excitation. These two observations are characteristic of a NL system.

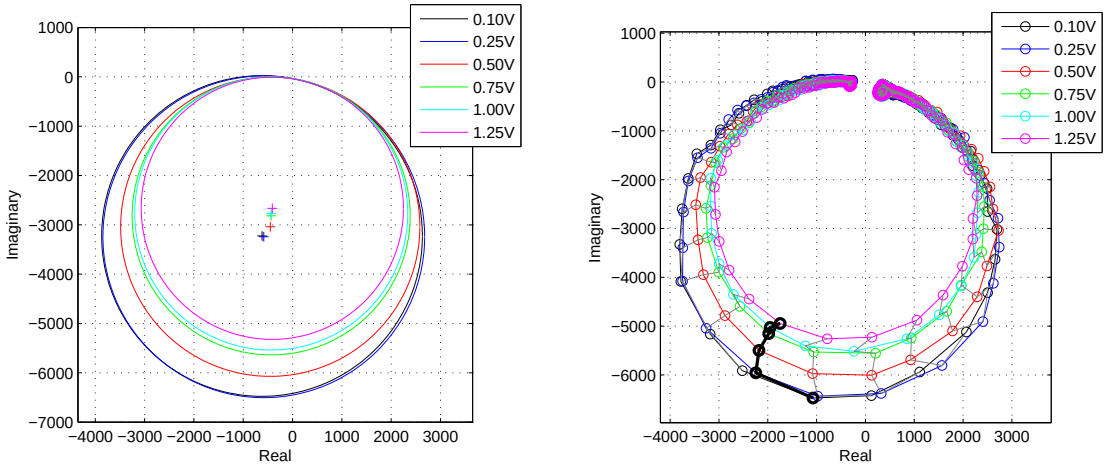

(a) Circle-fitted Nyquist (b) Nyquist with frequency points connected

Figure 3.4: Beam Nyquist plots

3.2 Variations on Double Beam Design

Two variations were made to the double beam device to see the effects on the response. One change made was to place square rubber partitions in between the two beams and in between the lower beam and aluminium cube. This was done to assess the importance of the friction at the interface. By changing the material at the interface it both changes the coefficient of friction at the interfaces and adds a softer, more flexible interface. The second variation made was to insert sections of wire into the semicircular extrusions in the beams. In doing this the stiffness of the beams is altered and the beam stiffness is no longer a homogeneous property. Fig. 3.5 compares the receptances of the two variations with the original response at 1V excitation level in the frequency range 100 Hz to 300 Hz. It is evident that the wire inserts made a much smaller difference to the response compared with the rubber partitions. The wire inserts caused the peak amplitude and the natural frequency to reduce while maintaining the same shaped peak. The rubber partitions resulted in the natural frequency being significantly lower, the peak amplitude diminishing and the shape of the peak became much broader.

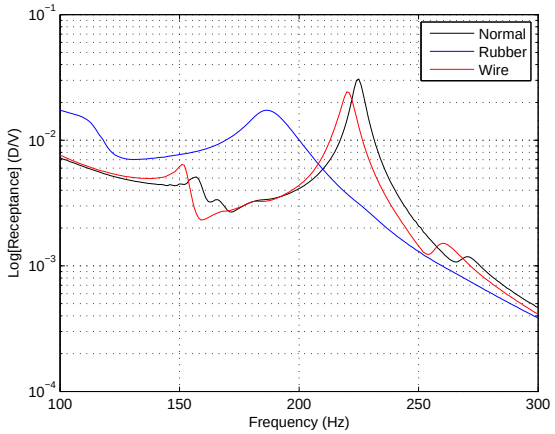

Figure 3.5: Double beam variants' receptances

Fig. 3.6 shows the responses at different excitation levels of the two variations on the double beam device. The graphs are normalised by the response with the greatest amplitude - 0.1V. Both responses experience smaller resonant peaks as the input voltage is increased. The response of the double beam with rubber partitions experiences a lower natural frequency as input voltage increases while the device with wire inserts has a spine which is almost vertical.

The explicit relationships of natural frequency vs input voltage and peak amplitude vs input voltage are graphed in Fig. 3.7 (a) and (b) respectively. The relationship for all three device set-ups are compared on each graph. The trend of the natural frequency vs input voltage graph for the wire inserts is identical to original device while the rubber partitions result in much lower natural frequencies and a consistent downwards trend. There is a 3.1% change in the natural frequency between 0.10v and 3.00V excitation for the device with rubber partitions. There is a 34.6Hz difference between the mean average natural frequency of the rubber partitioned device compared and the original device while there is only a 4.5Hz difference between the natural frequencies of the other two devices. The peak amplitudes all show an apparent exponential

decay as input voltage increases, with the rubber partitions causing the lowest peaks.

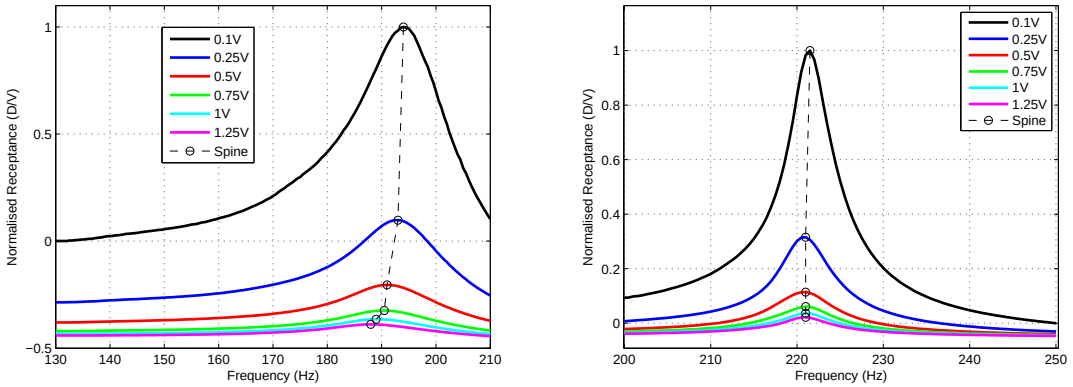

(a) Double beam with with rubber partitions (b) Double beam with wire inserts

Figure 3.6: Double beam variants' receptances

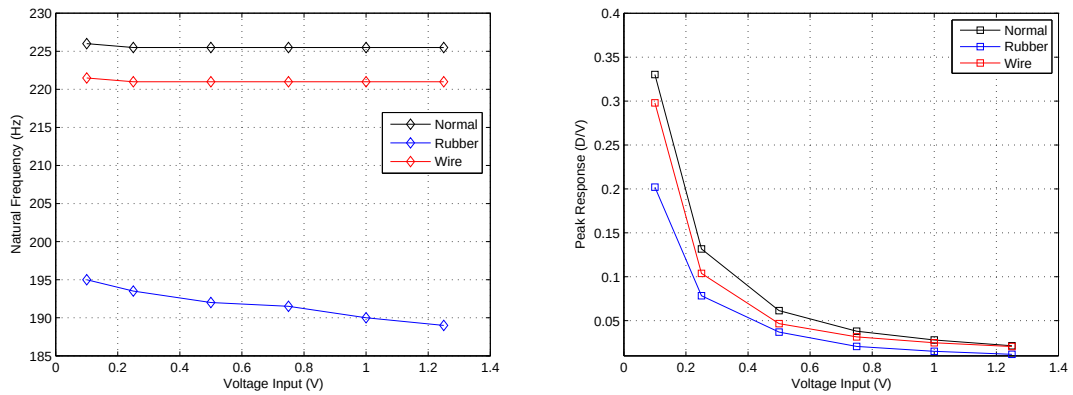

(a) Natural frequency vs voltage (b) Peak amplitude vs voltage

Figure 3.7: Beam variations comparison

3.3 Ring and Pillar Design

Fig. 3.8 shows the response at different levels of excitation of the ring and pillar device for both an up-step and a down-step experiment. For the up-step a 1DOF linear estimation has been fitted by the same means as for the double beam device. It is evident that the linear natural frequency is even higher than 0.25 V response. Both plots exhibit smaller response peaks and a shift to lower natural frequencies (reduced stiffness) as input voltage is increased. The up-step experiences an increase in natural frequency as voltage increases from 2.00 V to 3.00 V. The up-step, in general, has higher response peaks compared with the down-step response (Fig. 3.9 (d)).

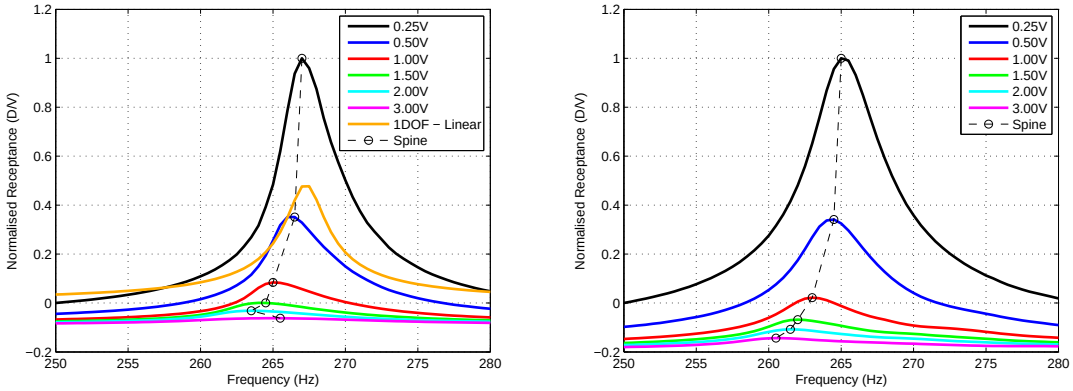

(a) Ring and pillar step-up signal receptance

(b) Ring and pillar step-down receptance

Figure 3.8: Ring and pillar forwards and backwards receptances 250 Hz to 280 Hz

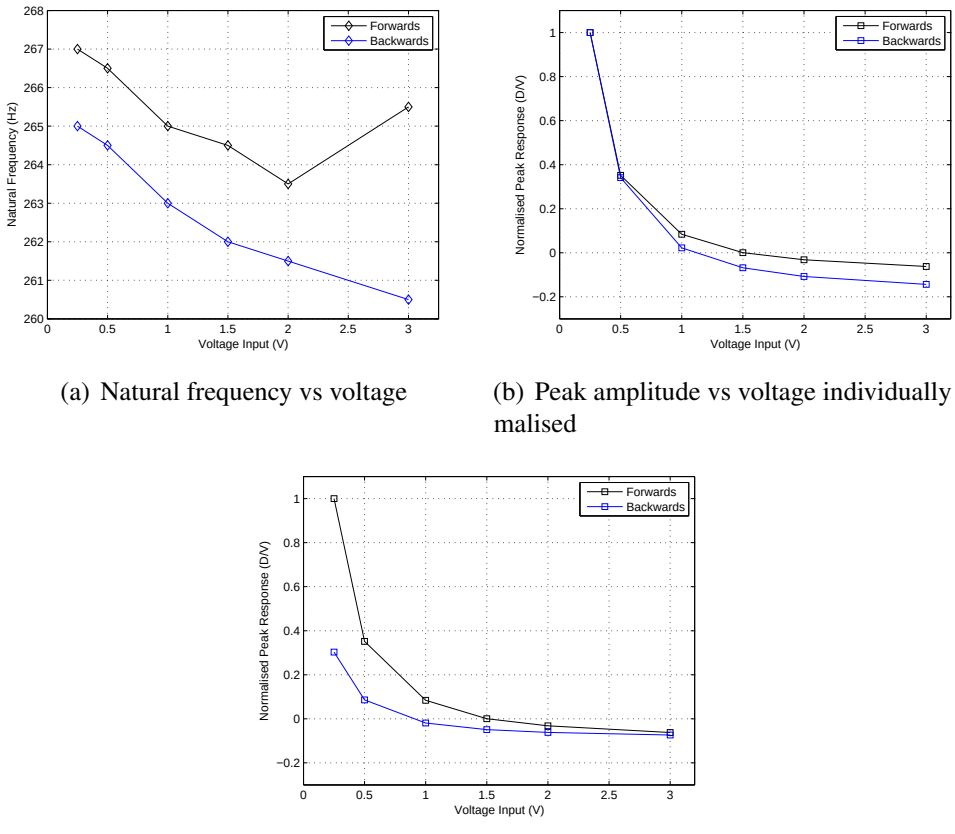

(a) Natural frequency vs voltage

(b) Peak amplitude vs voltage individually normalised

(c) Peak amplitude vs voltage both normalised by up-step response

Figure 3.9: Ring and pillar forwards vs backwards analysis 250 Hz to 280 Hz

Fig. 3.9 compares the response of the device when subjected to up-step and down-step excitation. The natural frequencies, while lower for the down-step, follow the same downwards trend until the input voltage reaches 3.00 V. To assess whether this is an anomalous point or not would need further investigation into the input voltage range of 2.00 V to 3.00 V. The difference in the mean average natural frequency between the two directions of sweep is 2.1 Hz (excluding the two last points at 3.00 V excitation). The peak amplitude graphs have each been normalised independently. In doing this the progressive reduction in peak amplitude can be assessed for each set of data (forwards and backwards sweep) and then compared with the other. It is evident that the peak amplitude of the backwards sweeping responses diminishes quicker than the forwards sweeping response.

The Nyquist plots given for the ring and pillar device (Fig. 3.10) give a clear view of the circle fits on even axes reducing in magnitude as input voltage goes from 0.25 V to 3.00 V. There is also a much more distinguished presence of the lines connecting the frequency points on each Nyquist plot not fitting a straight line and hence showing the existence of non-linearity - the frequency points rotate clockwise around the Nyquist plot and the plots reduce in magnitude as input voltage is increased. The 265.5 Hz frequency point is taken to demonstrate the rotation of the point around the centre of Nyquist plots.

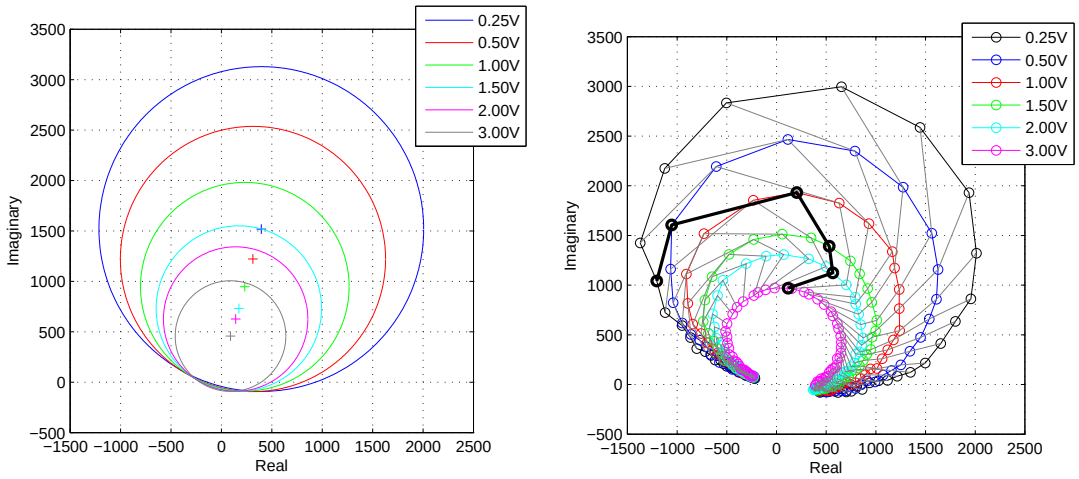

(a) Circle-fitted Nyquist

(b) Nyquist with frequency points connected

Figure 3.10: Ring Nyquist plots

4 Discussion

Both devices displayed NL behaviour which is visible from the FRFs and Nyquist plots plotted from the experimental data. The evidence of the NL properties are listed below for each device.

Double Beam Device

- Reduced resonant peak as input voltage is increased
- A higher natural frequency for 0.1V input voltage
- Non-circular Nyquist plots
- Rotation of frequency points about the centre of the Nyquist plot

Variations

- Similar response to the original device when wire inserts added
- When the rubber partitions were added, the natural frequency reduced significantly for 1V excitation compared with the original device and the natural frequency reduced noticeably as input voltage was increased.

Ring and Pillar Deivce

- Reduced resonant peak as input voltage is increased
- The natural frequency reduced as input voltage was increased
- Non-circular Nyquist plots
- Rotation of frequency points about the centre of the Nyquist plot
- The backwards step exhibited a different response to the forwards step.

4.1 Double Beam Device

The natural frequencies estimated by the FEM model for the double beam device are 10.7%(249.7 Hz) and 13.3%(255.5 Hz) higher than the natural frequency found experimentally - 225.5 Hz. By investigating the response at lower excitation voltages it is possible that the device stiffness would continue to harden and this gap between the model and the experimental results would close (but only marginally). One reason for this discrepancy could be that the contact area between the parts was modelled as being constrained from any translation, rotation or separation instead of being modelled as a bolted connection. In reality the faces are not constrained in this way; they may separate momentarily and slide relative to one another during excitation. Another reason for this discrepancy in natural frequency could be the limitations of FEM. Firstly, an FEM model, in theory, gets increasingly accurate as the mesh gets increasingly fine, and so would need infinitesimally small elements to be perfectly accurate. Secondly, while being able to model NL materials, it doesn't model linear materials in a NL manner, thus the FEM model is a linear model compared with the experimental results.

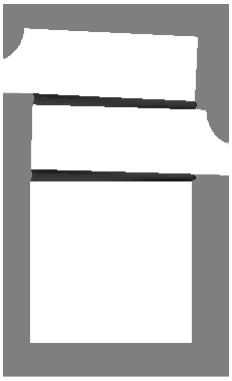

Figure 4.1: Central column with rubber: front view

The original device's response closely replicates a linear response, with exception to the fact that the peaks appear to decay exponentially as the level of excitation increases. This is as a result of the coulomb friction at the joint. As the device is excited, slip begins to occur in the joint. As slip occurs, friction at the interfaces of the parts produces increased damping in the device. Thus as force is increased, more slip occurs, which is turn results in higher damping.

The variations made to the double beam device help to discern the primary source of non-linearities. The wire inserts change the stiffness of the beam, both changing its value and making it inhomogeneous. The rubber partitions change the dynamics at the interface, adjusting both the coefficient of friction and the rigidity of the contact. Inserting the wire into the semicircular extrusions only changed the response marginally, while the rubber partitions affected the response much more drastically. They reduced the response peak and natural frequency for 1 V input voltage (Fig. 3.5) while also reducing the natural frequency as input voltage was increased (Fig. 3.7). From this statement it is evident that the device is more sensitive to adjustments at the interfaces of the parts and it is suggested the primary location of non-linearity for the double beam device is present at the interface of the parts. By changing the material combination at the interface the coefficient of friction, μ, changes from 1.05-1.35 to 0.6-0.7 and is likely that there are changes the undefined coefficients of higher and lower order terms in Eq. 4. Changing the interface to a softer and more elastic material will result in less separation of the adjacent faces. This is due to a higher poisson ratio found in rubber which creates a more pliable material. It may be seen in Fig. 4.1 that the rubber changes shape dependant on the relative position of the two beams. It is evident that the rubber partitions result in a spine which displays softening behaviour as peak amplitude decreases. This may be explained by the fact that rubber (just as can be found from a simple Hooke's Law experiment with elastic bands) have a spring constant, k, which is inherently NL. Thus as the rubber is compressed further at higher resonant peaks it becomes harder, conversely, for lower resonant peaks, it is relatively softer and hence the natural frequency reduces according to $\omega_n = \sqrt{\frac{k}{M}}$ as can be seen in Fig. 3.7.

Roth et al. (1942) makes two assertions about the coefficient of friction in rubber, as sliding speed increases, so does μ, and vibration during experiments results in a lower friction coefficient. Thus it can be assumed that due to the vibration the friction coefficient between the aluminium and the rubber is less than 0.6. From this it is evident that greater slip will occur at any given

excitation voltage, which will result in higher overall damping and thus lower resonant peaks. This can be seen in Fig. 3.5 where the resonant peak of the device with the rubber partitions is much lower than those without. As for all cases with the double beam device the response diminishes due to increased damping as friction ensues as a result of slip.

4.2 Ring and Pillar

For the ring and pillar device the natural frequency estimated by the FEM model is only 2% lower than the experimentally found natural frequency. This is an accurate estimation but would be sufficiently close in industry for projects with low levels of safety risk, particularly when considering that safety factors are included into design processes as a general practice. The constraints for modelling bolts was used for the ring and pillar device as for the double beam device. The peak response amplitude reduced for the higher levels of excitation, which can be explained by coulomb friction at the joint as the surfaces slide relative to each other under excitation. The softening behaviour displayed by the spine of the FRF can be said to be due to the arches. These arches act as springs, when the peak resonance is higher, there is greater displacement resulting in a hardening of the 'spring'. Conversely, as peak amplitude reduces the spring softens and the natural frequency reduces, as can be seen in Fig. 3.9.

The inspection of path dependency by comparing the response due to an up-step with the response due to a down-step showed that the response was path dependant. From this statement it is clear that in industry parts must be designed with all forms of excitation in mind. For example, when a structure is excited by wind, it may not resonate as the wind increases in force and speed, however, as the wind force reduces when the storm settles, the structure may resonate.

5 Conclusion

From comparison of experimental results with linear theory, it has been extensively shown that both devices exhibit NL behaviour. This was done using FRFs and Nyquist plots to demonstrate the properties of the plots which characterise NL behaviour.

The double beam device was used to show how varying a device can be used to both localise the source of non-linearities and increase the extent to which a structure is NL. The original device had a spine which neither lent forwards nor backwards, showing no softening or hardening behaviour, however, the reduced resonant peak as voltage increased signified an increase in damping. The frequency points on the Nyquist plots changed phase as voltage input varied, signifying a change in phase for a given frequency.

The ring and pillar device was used to demonstrate the effects of path dependency through comparing up-step and down-step responses. While both responses decreases in magnitude and natural frequency as input voltage increased, the down-step response had smaller amplitudes and reduced at a quicker rate as input voltage was increased compared with the up-step. Along with this, the natural frequency for each excitation level was lower for the down-step response.

In both devices the peak amplitudes reduced as input voltage increased as a result of coulomb friction at the bolted joints. As the interfaces began to slide, the friction caused increase damping. The softening behaviour demonstrated by the shape of the spine in the double beam device with rubber partitions and the ring and pillar device was due to the same principle manifesting itself in two different ways. For the double beam device it was the rubber which has NL stiffness properties as it is compressed while in the ring and pillar device it was the arches which acted as springs. When these springs were displaced sufficiently the springs became NL.

5.1 Future Work

Further work to be done on this project could include:

- Assess the other natural frequencies of the double beam device: 150 Hz to 180 Hz and 250 Hz to 280 Hz;
- Investigate lower excitation frequencies for the double beam device to see if the spine begins to show hardening or softening behaviour;
- Determine whether the apparently anomalous point in Fig. 3.9 (a) is indeed anomalous by testing for at more excitation voltages in the range of 2.00 V to 3.50 V;
- Accept or reject the hypothesis that the double beam model estimates for the natural frequency determined by the FEM software was wrong due to the inaccurate modelling of the bolted joint by remodelling both device with bolted connections;
- Document the analysis of the variations made to the ring and pillar device and the comparison of the up- and down-step responses of the double beam device to complete the analysis for each model;

- Conduct force-displacement graphs for the arches in the ring and pillar device and force-compression graphs for the rubber used for rubber partitions.

Future work to build on this project:

- Investigate the two devices in a more quantitative domain, determining the form and coefficients of non-linearity (as suggested by Kerschen et al. (2005) in Fig. 1.2) for each device. This could be done using methods discussed in the literature review, with particular reference to Siller (2004), Eriten et al. (2013) and Kerschen et al. (2005).

References

Aalco. Aluminium alloy - commercial alloy - 6082 - t6 extrusions. [ONLINE] Available at: http://www.aalco.co.uk/datasheets/Aluminium-Alloy-6082-T6-Extrusions_338.ashx. [Accessed 08 March 15], 2013.

M. Amabili. Nonlinear vibrations of rectangular plates with different boundary conditions: theory and experiments. *Computers and Structures*, 2004.

M. Eriten, M. Kurt, G. Luo, d. Michael McFarland, L. A. Bergman, and A. F. Vakakis. Nonlinear system indentification of frictional effects in a beam with a bolted joint connection. *Mechanical Systems and Signal Processing*, 2013.

D. J. Ewins. *Modal Testing, Theory, Practice, and Application*. Research Studies Press Ltd., 2nd edition, September 2000.

W. Gander, G. H. Golub, and R. Strebel. Least-sqaures fitting of circles and ellipses. Technical report, Institut fur Wissenschaftliches Rechen and Stanford University.

G. Kerschen, K. Worden, A. F. Vakikis, and J. Golinval. Past, present and future of nonlinear system identification in structural dynamics. *Mechanical Systems and Signal Processing*, 2005.

D. C. Lagoudas, L. G. Machado, and M. Z. Lagoudas. Nonlinear vibration of a one-degree of freedom shape memory alloy oscillator: A numerical-experimental investigation. Technical report, Texas A&M University and Spacecraft Technology Center, 2005.

M. Link, M. Boeswald, S. Laborde, M.Weiland, and A. Calvi. Non-linear experimental modal analysis and application to satellite vivbration test data. In *Computational Methods in Structural Dynamics and Earthquake Engineering*, 2011.

C. McMahon. Product development models and standards. Product Design Course notes, 2014.

F. L. Roth, R. L. Driscoll, and W. L. Holt. Frictional properties of rubber. *Journal of Research of the National Bureau of Standards*, 28, April 1942.

H. R. E. Siller. *Non-linear Modal Analysis Methods for Engineering Structures*. PhD thesis, Imperial College London, University of London, August 2004.

P. Wilcox. Nonlinear analysis. FEA Lecture course handout, 2014.

Appendices

List of Equipment

- Labview Software
- Two Single Degree of Freedom Accelerometers (sensitivities 98.5mV/g and 96.5mV/g)
- Signal Amplifier
- Derritron VP4 Shaker Table
- Kistler Box
- National Instruments 6211 AO/AI DAQ Junction Box

Comparison of two sensors' response

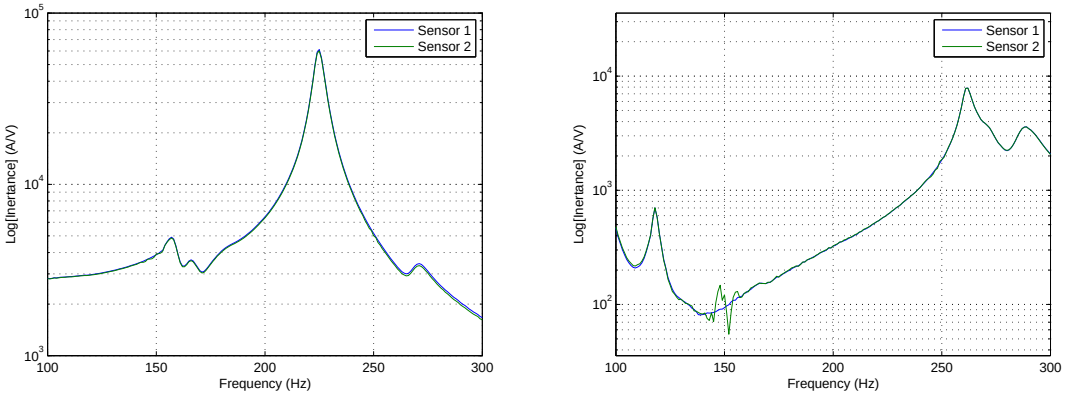

(a) Double Beam Set-up

(b) Ring and Beam Set-up

Figure 5.1: Comparison of Two Sensors' FRFs at 1 V, 100 Hz to 300 Hz

Full set of Nyquist Plots

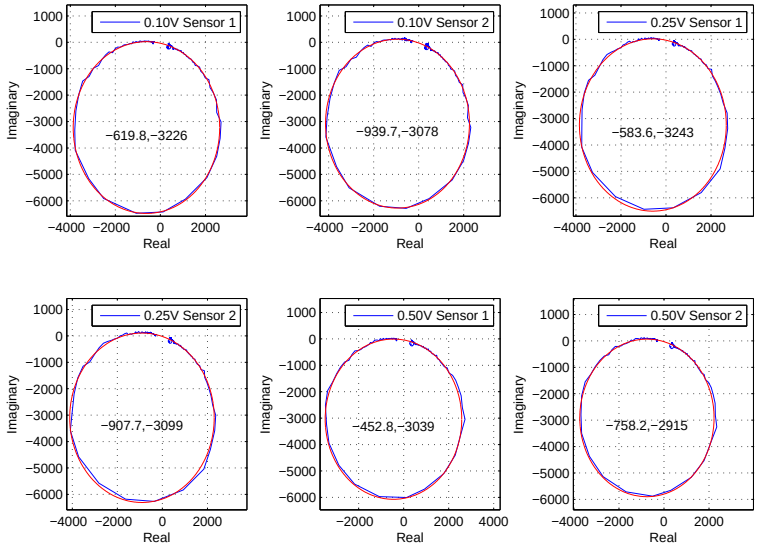

Figure 5.2: Double beam Nyquist plots 0.10 V to 0.50 V

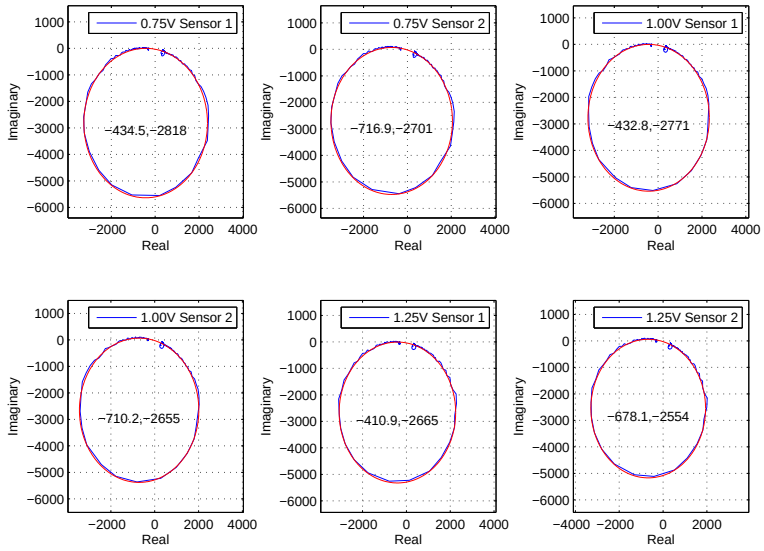

Figure 5.3: Double beam Nyquist plots 0.75 V to 1.25 V

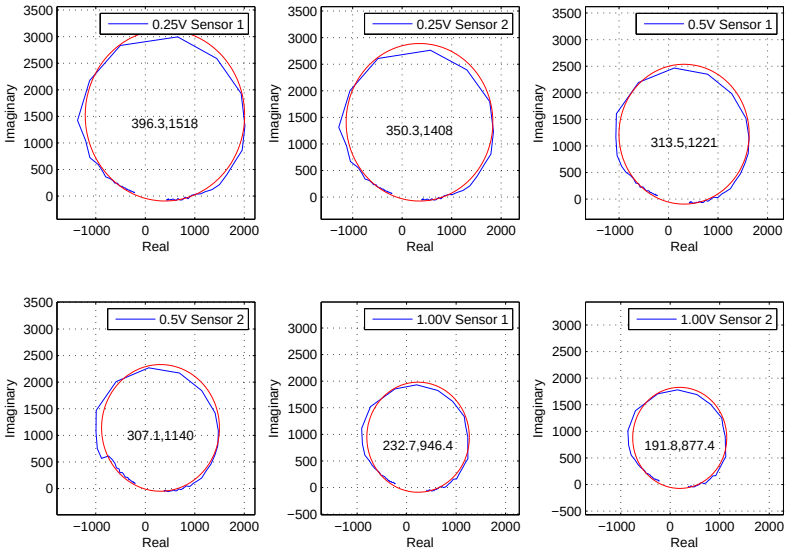

Figure 5.4: Ring and pillar Nyquist plots 0.25 V to 1.00 V

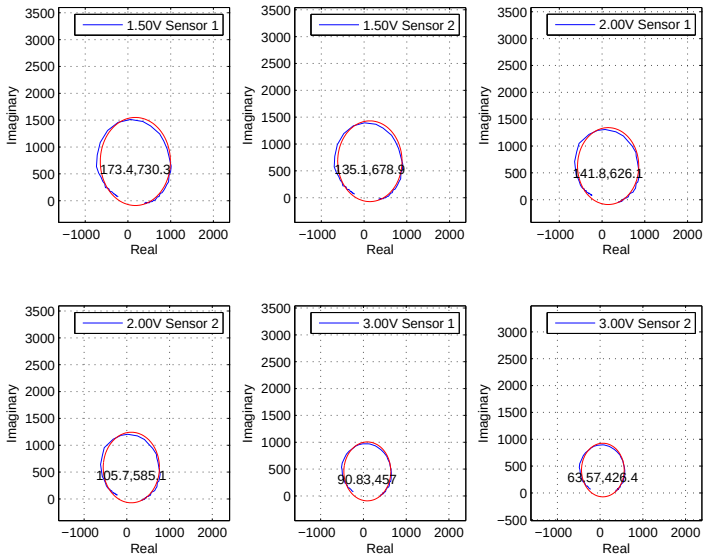

Figure 5.5: Ring and pillar Nyquist plots 1.50 V to 3.00 V